communications earth & environment

ARTICLE

https://doi.org/10.1038/s43247-022-00485-8 OPEN

Intracellular nitrate storage by diatoms can be an important nitrogen pool in freshwater and marine ecosystems

Peter Stief[1,2✉], Clemens Schauberger[2], Marie B. Lund[3], Andreas Greve[1], Raeid M. M. Abed[1,4], Mohammad A. A. Al-Najjar[1,5], Karl Attard[2,6], Stefano Bonaglia[2,7], Jörg S. Deutzmann[8], Belén Franco-Cisterna[2], Emilio García-Robledo[9], Moritz Holtappels[10], Uwe John[10,11], Adele Maciute[7], Michael J. Magee[2], Rie Pors[2], Tina Santl-Temkiv[3], Anja Scherwass[12], Duygu S. Sevilgen[1,10], Dirk de Beer[1], Ronnie N. Glud[2,6,13], Andreas Schramm[3] & Anja Kamp[1,3,14]

Identifying and quantifying nitrogen pools is essential for understanding the nitrogen cycle in aquatic ecosystems. The ubiquitous diatoms represent an overlooked nitrate pool as they can accumulate nitrate intracellularly and utilize it for nitrogen assimilation, dissipation of excess photosynthetic energy, and Dissimilatory Nitrate Reduction to Ammonium (DNRA). Here, we document the global co-occurrence of diatoms and intracellular nitrate in phototrophic microbial communities in freshwater ($n = 69$), coastal ($n = 44$), and open marine ($n = 4$) habitats. Diatom abundance and total intracellular nitrate contents in water columns, sediments, microbial mats, and epilithic biofilms were highly significantly correlated. In contrast, diatom community composition had only a marginal influence on total intracellular nitrate contents. Nitrate concentrations inside diatom cells exceeded ambient nitrate concentrations ~100–4000-fold. The collective intracellular nitrate pool of the diatom community accounted for <1% of total nitrate in pelagic habitats and 65–95% in benthic habitats. Accordingly, nitrate-storing diatoms are emerging as significant contributors to benthic nitrogen cycling, in particular through Dissimilatory Nitrate Reduction to Ammonium activity under anoxic conditions.

[1] Microsensor Group, Max Planck Institute for Marine Microbiology, 28359 Bremen, Germany. [2] Department of Biology, HADAL & Nordcee, University of Southern Denmark, 5230 Odense M, Denmark. [3] Department of Biology, CEM & Section for Microbiology, Aarhus University, 8000 Aarhus C, Denmark. [4] Department of Biology, Sultan Qaboos University, 123 Muscat, Oman. [5] Faculty of Pharmacy, Applied Science Private University, 11391 Amman, Jordan. [6] Danish Institute for Advanced Study, University of Southern Denmark, 5230 Odense M, Denmark. [7] Department of Marine Sciences, University of Gothenburg, 41319 Gothenburg, Sweden. [8] Civil & Environmental Engineering, Stanford University, Stanford, CA 94305, USA. [9] Department of Biology, University of Cadiz, 11510 Cadiz, Spain. [10] Alfred-Wegener-Institute, 27570 Bremerhaven, Germany. [11] Helmholtz Institute for Functional Marine Biodiversity, 26129 Oldenburg, Germany. [12] Institute for Zoology, General Ecology, University of Cologne, Köln, Germany. [13] Tokyo University of Marine Science and Technology, 108-8477 Tokyo, Japan. [14] AIAS, Aarhus Institute of Advanced Studies, Aarhus University, 8000 Aarhus C, Denmark. ✉email: peterstief@biology.sdu.dk

Microorganisms involved in aquatic nitrogen cycling typically exploit freely dissolved inorganic nitrogen species, such as nitrate, nitrite, and ammonium, for the different nitrogen-cycle pathways[1]. The distribution of freely dissolved nitrogen pools within aquatic ecosystems thus often reflects the distribution and activity of the different nitrogen-cycle pathways and vice versa[2,3]. Some aquatic microorganisms, however, can accumulate and store nitrate in cell vacuoles at concentrations exceeding ambient concentrations by several orders of magnitude[4–6]. It is commonly believed that intracellular nitrate ($ICNO_3$) is utilized for nitrogen assimilation (N-assimilation) by phototrophic eukaryotes, such as diatoms[7,8], and for energy conservation through dissimilatory nitrate reduction by sulfide-oxidizing prokaryotes[5,9,10]. This paradigm was shattered by the discovery that several groups of marine microbial eukaryotes also utilize $ICNO_3$ for dissimilatory nitrate reduction, i.e., foraminifers[11], diatoms[12], fungi[13], and gromiids[14]. Diatoms can utilize $ICNO_3$ for Dissimilatory Nitrate Reduction to Ammonium (DNRA) to survive dark and anoxic conditions[12].

Since nitrate uptake in excess of immediate nutritional demands (i.e., "luxury uptake") occurs against a steep concentration gradient, it requires an energy investment[5,15]. In turn, nitrate storage conveys a competitive advantage in environments where the supply of nitrate is scarce, spatially confined, or temporally variable[16]. Nitrate uptake and intracellular storage in nitrate-replete subsurface layers allows survival and growth of migrating diatoms in nitrate-depleted surface layers of the ocean[17]. In benthic habitats with spatially separated electron acceptors (e.g., oxygen and nitrate) and donors (e.g., organic substrates and sulfide), nitrate-storing sulfur bacteria thrive by displaying vertical migration behavior between surface and subsurface layers[4,18]. Diel vertical migration behavior enabled by $ICNO_3$ storage and DNRA activity was only recently demonstrated for benthic diatoms[19].

Diatoms are ubiquitous in shallow freshwater and marine ecosystems where they often dominate phototrophic microbial communities in both pelagic and benthic habitats[20–23]. The ability to store nitrate intracellularly has been demonstrated for several diatom isolates and pelagic diatom communities[8,12,24–27], but not in a comprehensive way for the extensive diatom communities in sediments, microbial mats, and biofilms. Thus, the distribution and extent of $ICNO_3$ storage by diatom communities within and across diverse aquatic ecosystems remains unexplored. Knowing the distribution and size of diatom-specific $ICNO_3$ pools can serve as the basis to gauge the influence by diatoms on aquatic nitrogen cycling. Three nitrate-fueled nitrogen-cycle pathways have been described for diatoms so far, N-assimilation[7,8], nitrate reduction for dissipating excess photosynthetic energy (NRphot)[8,28–30], and DNRA under anoxic conditions[12,19].

Aside from fueling different nitrogen-cycle pathways, nitrate-storing diatoms may represent a significant local sink of freely dissolved nitrate ($FDNO_3$) in sediments and microbial mats. Efficient $ICNO_3$ storage keeps porewater nitrate concentrations low and thereby increases the diffusive flux of nitrate from adjacent sources (e.g., the water column), which influences nitrate availability for the entire benthic habitat. The local sink of $FDNO_3$ is decoupled in space and time from the ultimate diatom-mediated $ICNO_3$ turnover and thus from the uptake/release of other involved reactive compounds (e.g., ammonium, dissolved inorganic carbon). High diatom abundances may thus lead to misinterpretation of porewater profiles and incorrect rate calculations of nitrogen-cycle pathways in benthic habitats, which should be corrected for by biogeochemical modeling that takes $ICNO_3$ storage into account.

We studied the co-occurrence of diatoms and $ICNO_3$ in phototrophic microbial communities sampled in 117 globally distributed marine and freshwater habitat types (i.e., water column, sediment, microbial mat, and epilithic biofilm). We hypothesized that high diatom abundance coincides with high total $ICNO_3$ contents in space (vertical profiling) and time (seasonal monitoring). The role of diatom community composition for the prevalence of $ICNO_3$ storage was assessed via 18S rRNA gene amplicon sequencing. The rich dataset provided here revealed that habitat type and diatom abundance are key determinants for total $ICNO_3$ contents within aquatic ecosystems, while diatom community composition is of marginal importance. In benthic habitats, most of the total nitrate pool may indeed occur as intracellular nitrate stored by diatoms, suggesting that benthic nitrogen cycling is strongly influenced by diatoms.

Results

Global distribution of intracellular nitrate. A snapshot survey of phototrophic microbial communities was carried out in 117 globally distributed freshwater (69 sites) and marine (48 sites) habitats (Fig. 1, Supplementary Table 1, Supplementary Data 1). Four different habitat types were sampled: water columns (16 sites), sediments (43 sites), microbial mats (22 sites), and epilithic biofilms (36 sites). Open-ocean water column samples are underrepresented in this survey (4 sites). All samples from the snapshot survey were routinely analyzed for photopigments, $ICNO_3$, and freely dissolved nitrate ($FDNO_3$). In two sample subsets, diatom abundance and biovolume (Supplementary Table 2 and Supplementary Data 2), as well as diatom community composition (Supplementary Table 3 and Supplementary Data 3) were determined.

Habitat type. Total $ICNO_3$ contents spanned seven orders of magnitude across all habitat types, from very low levels in water columns to very high levels in epilithic biofilms (Fig. 2 and Supplementary Data 5). $ICNO_3$ contents were significantly correlated with chlorophyll *a* contents across all habitat types (Supplementary Fig. 1A, $R^2 = 0.799$, $p < 0.001$, $n = 654$), suggesting a role of phototrophic microorganisms in $ICNO_3$ storage. $ICNO_3$ contents were even more tightly correlated with fucoxanthin contents across all habitat types (Fig. 2, $R^2 = 0.864$, $p < 0.001$, $n = 654$), which is described by the power function $ICNO_3 = 3.77 \pm 1.06 \times Fucoxanthin^{0.753 \pm 0.013}$ (means ± standard error). In turn, fucoxanthin contents were significantly correlated with diatom cell abundance as determined microscopically in a subset of samples (Supplementary Fig. 2, $R^2 = 0.954$, $p < 0.001$, $n = 78$). These correlations suggest that diatoms are important for $ICNO_3$ storage in phototrophic microbial communities and that fucoxanthin contents can be used as a proxy for the abundance of nitrate-storing diatoms.

However, fucoxanthin also occurs in Dinophyceae, Prymnesiophyceae, Chrysophyceae, and Pelagophyceae. Published and newly added data indicate that these microalgal classes store intracellular nitrate at negligible concentrations compared to diatoms (Table 1, Supplementary Table 4, Supplementary Data 4). Additionally, the quantification of several marker pigments in this survey revealed that the relative abundance of the respective microalgal class was not positively correlated with total $ICNO_3$ contents across all habitat types (Supplementary Table 5). Low nitrate storage capacity and lack of correlation between relative abundance and total $ICNO_3$ contents were also found in microalgal classes that do not contain fucoxanthin, i.e., Cryptophyceae, Chlorophyceae, and the prokaryotic cyanobacteria (Table 1, Supplementary Tables 4 and 5). Microalgal classes other than diatoms and cyanobacteria are thus unlikely to contribute substantially to total $ICNO_3$ contents in aquatic habitats.

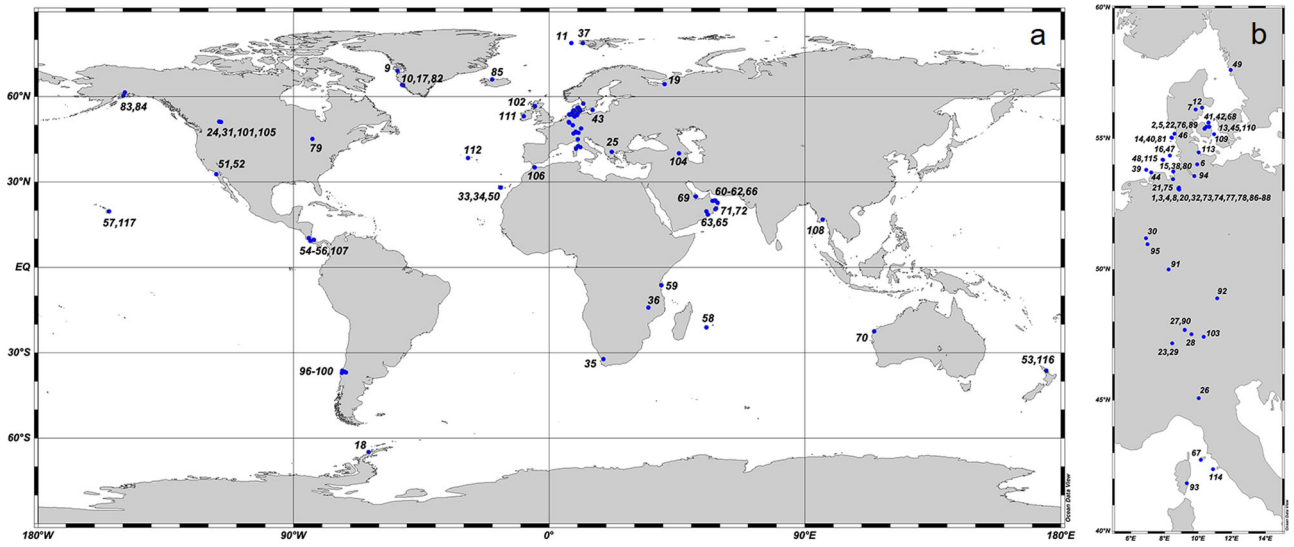

Fig. 1 Map of sampling sites. a Global and **b** Central European distribution of 117 sampling sites (numbered blue circles) at which the occurrence and the determinants of intracellular nitrate were studied. The map was created using the software package ODV 5.6.1 (Schlitzer, Reiner, Ocean Data View, odv.awi.de, 2021). Sampling details are given in Supplementary Table 1 (Supplementary Data 1) and in an interactive map created using Google My Maps (https://bit.ly/2XF9kkQ).

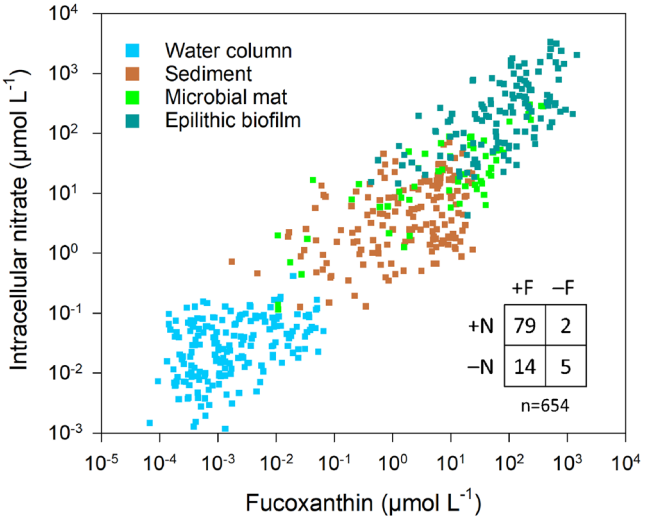

Fig. 2 Global distribution of intracellular nitrate. Overall correlation between intracellular nitrate ($ICNO_3$) and fucoxanthin (a diatom marker pigment) across habitat types and climate zones. Total $ICNO_3$ and fucoxanthin contents are expressed per unit volume of the respective habitat. The correlation is described by the power function: $ICNO_3$ (µmol L^{-1}) = 3.77 × Fucoxanthin (µmol L^{-1})$^{0.75}$ ($R^2 = 0.864$, $p < 0.001$, $n = 654$). Inset shows frequency distribution (in %) of samples in which intracellular nitrate (N) and fucoxanthin (F) were detected (+) or not detected (-).

In contrast, the quantitative relationship between $ICNO_3$ and diatoms is substantiated by finding that $ICNO_3$ and fucoxanthin contents were also correlated within each habitat type (Supplementary Table 6) and that total $ICNO_3$ contents were positively correlated with the fucoxanthin/chlorophyll *a* ratio (i.e., a proxy for relative diatom abundance) (Supplementary Fig. 1B and Supplementary Table 6). Additionally, most samples (79%) harbored both $ICNO_3$ and fucoxanthin, while samples harboring $ICNO_3$ but lacking fucoxanthin were rare (2%) (Fig. 2).

Table 1 Intracellular nitrate storage capacity by different microalgal classes.

Microalgal class	Fucoxanthin	Cell volume (µm^3)	$ICNO_3$ (mmol L^{-1})	$ICNO_3$ (fmol $cell^{-1}$)
Bacillariophyceae (Diatoms)	YES	3226	40.8	131.6
Dinophyceae	YES	12141	0.3	4.1
Chrysophyceae	YES	107	5.5	0.6
Prymnesiophyceae	YES	205	0.0	0.0
Pelagophyceae	YES	5	n.d.	n.d.
Cryptophyceae	NO	217	1.8	0.4
Chlorophyceae	NO	422	0.4	0.2
Cyanobacteria	NO	174	n.d.	n.d.

Fucoxanthin YES/NO indicates that fucoxanthin occurs/does not occur in the respective microalgal class. The median cell volume of each microalgal class was calculated from data presented in the ICES report "PEG_BVOL_2021". The median $ICNO_3$ concentration of each microalgal class was calculated from published data and from data obtained in this study (Supplementary Table 4 and Supplementary Data 4). The median $ICNO_3$ content of each microalgal class was calculated from its median $ICNO_3$ concentration and cell volume. Note that the prokaryotic cyanobacteria are only functionally equivalent to the eukaryotic microalgae listed here. *n.d.* no data.

Freely dissolved nitrate. The influence of $FDNO_3$ concentrations on total $ICNO_3$ contents was ambiguous (Supplementary Fig. 3). Monotonic relationships across habitat types were neither observed for water column nitrate, nor for porewater nitrate ($PWNO_3$) (Supplementary Fig. 3A, B). However, significant, positive correlations were found for sediments and epilithic biofilms (Supplementary Table 6).

Diatom abundance and biovolume. For 6–8 sampling sites within each habitat type (Supplementary Table 2 and Supplementary Data 1), diatom cells were counted and sized by microscopy. Both diatom cell abundance and total diatom biovolume spanned 6–7 orders of magnitude across all habitat types, from very low values in water columns to very high values in mats and biofilms (Fig. 3a and Supplementary Data 6). Total $ICNO_3$ contents were highly significantly correlated with diatom cell abundance and total diatom biovolume across all habitat types (Fig. 3a, b, $R^2 = 0.823$

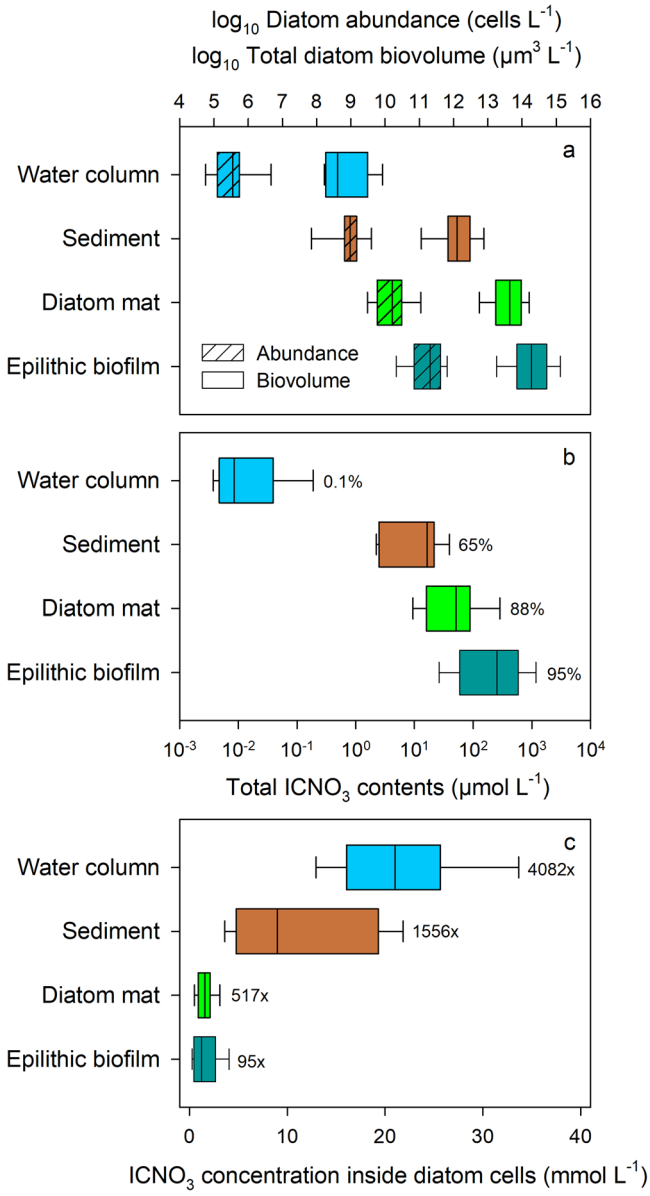

Fig. 3 Intracellular nitrate in diatom habitats and inside diatom cells. **a** Diatom abundance and total diatom biovolume, **b** total $ICNO_3$ contents, and **c** $ICNO_3$ concentration inside diatom cells in water columns (blue), sediments (brown), microbial mats (green), and epilithic biofilms (cyan). Note different units for $ICNO_3$ in **b**, **c**. Percent values in **b** give the median of the relative contribution of $ICNO_3$ to total nitrate in each habitat type. Multiplication factors in **c** give the median of the enrichment of $ICNO_3$ concentration inside diatom cells relative to freely dissolved nitrate ($FDNO_3$) concentration in each habitat type. Box plots show median (solid line), 25th and 75th percentiles (box), and 10th and 90th percentiles (whiskers) of $n_A = 6$–8 sampling sites within each habitat type and $n_B = 3$ replicates each.

and $R^2 = 0.899$, respectively, $p < 0.001$, $n = 84$) and also within most habitat types (Supplementary Table 6). This confirms that total fucoxanthin contents indeed reflected diatom cell abundance and total diatom biovolume in this survey.

The relative contribution of $ICNO_3$ to total nitrate in each sample was calculated as $ICNO_3/(ICNO_3 + FDNO_3)$ for water column samples and as $ICNO_3/(ICNO_3 + PWNO_3)$ for sediment, mat, and biofilm samples and expressed in percent. It turned out that $ICNO_3$ accounted for 0.1% of total nitrate in pelagic habitats and 65–95% in benthic habitats (Fig. 3b and Supplementary Data 6). Assuming that the total $ICNO_3$ contents were exclusively stored by diatoms, the average $ICNO_3$ concentration inside diatom cells ranged between 1.6 (diatom mats) and 21.8 mmol L^{-1} (water column) (Fig. 3c and Supplementary Data 6). Strikingly, the $ICNO_3$ concentrations inside diatom cells exceeded the respective $FDNO_3$ concentrations between 95- and 4082-fold in the different habitat types (Fig. 3c), again assuming that diatoms were the exclusive microorganisms storing $ICNO_3$ in these samples.

Vertical distribution of intracellular nitrate. In 16 vertically profiled aquatic habitats, the total $ICNO_3$ and photopigment contents were generally highest close to the sunlit surface and decreased with depth (Fig. 4, Supplementary Fig. 4, Supplementary Data 7). Fucoxanthin and $ICNO_3$ profiles had matching shapes on a meter (water column), centimeter (sediment), and millimeter scale (microbial mat). This was not the case for phycocyanin, a marker pigment for cyanobacteria, which can be abundant in microbial mats (Fig. 4g and Supplementary Fig. 4). In most sediments and microbial mats, the vertical profiles of $ICNO_3$ and $PWNO_3$ contents had similar shapes with clear surface maxima and very low levels at greater depth (Fig. 4 and Supplementary Fig. 4).

As an extreme case of microbial stratification, thin, golden-brown diatom layers were skimmed off sediment surfaces at nine sampling sites and analyzed separately (Supplementary Table 1 and Supplementary Data 1). Without exception, these "diatom mats" had very high total $ICNO_3$ and fucoxanthin contents. Similarly, epilithic biofilms were detached from the surface of sunlight-exposed stones and pebbles at 36 sampling sites (Supplementary Table 1 and Supplementary Data 1). Epilithic biofilms did not only display the highest average contents of $ICNO_3$ (476 µmol L^{-1}, $n = 134$) and fucoxanthin (192 µmol L^{-1}, $n = 139$), but also the single highest values of $ICNO_3$ (3329 µmol L^{-1}) and fucoxanthin (1451 µmol L^{-1}) of all samples analyzed in this survey.

Seasonal variation of intracellular nitrate. In the water column of four seasonally monitored aquatic habitats from the temperate zone, total chlorophyll *a*, fucoxanthin, and $ICNO_3$ contents showed one or two pronounced maxima during the warm season (Fig. 5 and Supplementary Data 8). $ICNO_3$ maxima coincided to a large extent with fucoxanthin maxima, i.e., with the appearance of diatom blooms. In contrast, total $ICNO_3$ and phycocyanin contents did not co-vary. Coinciding with the emerging spring blooms, $FDNO_3$ concentrations decreased and remained low during the warm season. Nevertheless, total $ICNO_3$ contents remained high, indicating that the low $FDNO_3$ concentrations did not limit nitrate uptake and $ICNO_3$ storage.

Diatom community composition. For 7–16 sampling sites within each habitat type (Supplementary Table 3 and Supplementary Data 3), diatoms were identified through 18S rRNA gene sequence analysis. In total, 43 out of 53 samples produced each >5000 sequence reads and were used for further analysis (Supplementary Table 3 and Supplementary Data 3). The ten samples excluded from further analysis produced <5000 sequence reads and corresponded without exception to samples with very low total $ICNO_3$ and fucoxanthin contents and diatom abundance. Based on relative sequence abundance, centric diatoms of the order Thalassiosirales (class Mediophyceae) dominated the communities in most water columns, while pennate diatoms of the order Naviculales (class Bacillariophyceae) dominated the communities in most sediment, mats, and biofilms (Fig. 6). Other abundant diatom orders in benthic habitats included Fragilariales

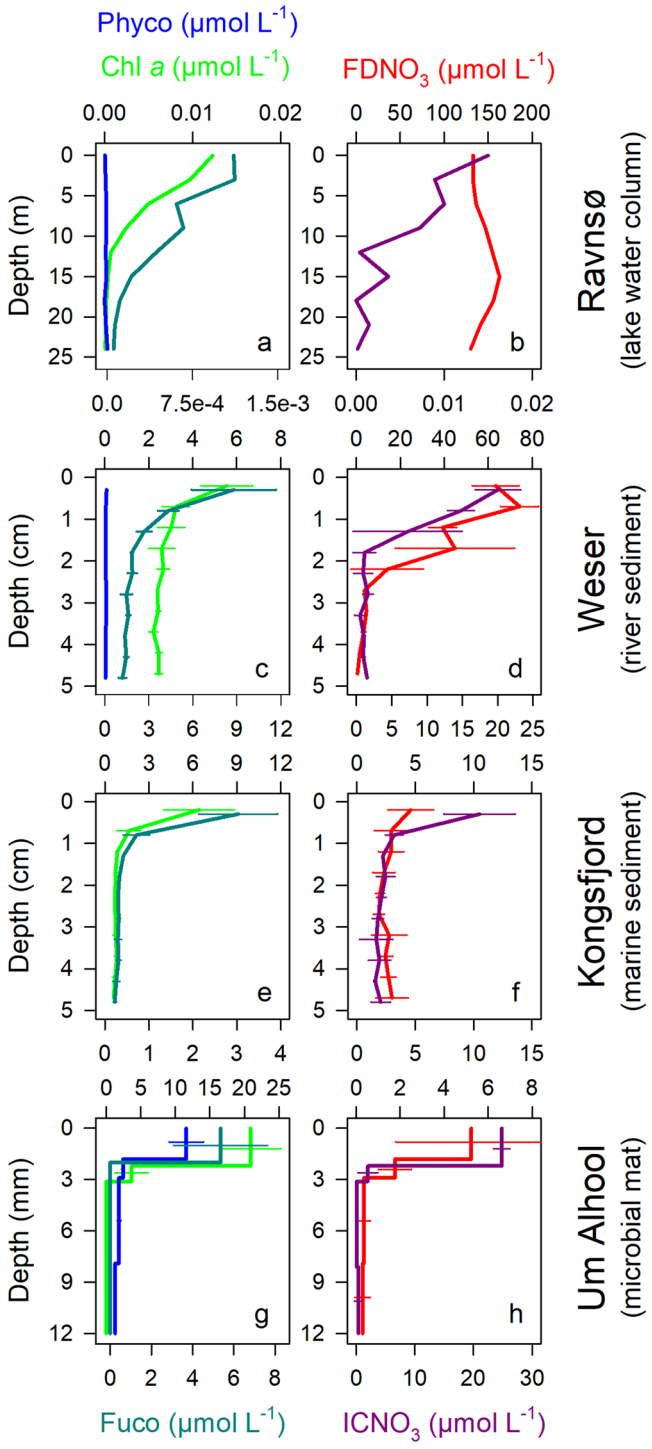

Fig. 4 Vertical distribution of intracellular nitrate. a, **c**, **e**, **g** Total contents of chlorophyll *a* (Chl *a*), fucoxanthin (Fuco), and phycocyanin (Phyco) (a cyanobacteria marker pigment) and **b**, **d**, **f**, **h** freely dissolved nitrate ($FDNO_3$) and intracellular nitrate ($ICNO_3$) in one lake water column, two sediments, and one microbial mat. For sediments and microbial mats, $FDNO_3$ refers to porewater nitrate. For Kongsfjord, no phycocyanin data are available. Note that *y*-axes have meter, centimeter, and millimeter scales for water column, sediment, and microbial mat, respectively. Means ± standard deviation of $n = 3$ are shown; for better visibility, vertical sampling points are slightly offset. Vertical profiles for twelve additional sampling sites are shown in Supplementary Fig. 4.

(sediments), Thalassiosirales and Bacillariales (diatom mats), and Achnanthales, Bacillariales, and Cymbellales (epilithic biofilms).

All habitat types had significantly different diatom communities (ANOSIM: $R = 0.274 \pm 0.079$, $p < 0.05$), except for sediments and diatom mats, which shared similar diatom communities (ANOSIM: $p > 0.05$) (Fig. 7 and Supplementary Table 7). There was also a significant difference in diatom community composition between marine and freshwater habitats (ANOSIM: $R = 0.53$, $p < 0.001$). Notably, the variation in total $ICNO_3$ contents was only marginally explained by dissimilarities of diatom communities (PERMANOVA: $R^2 = 0.04$, $p = 0.011$).

Discussion

Diatoms as widespread nitrate-storing microorganisms. Our results provide two lines of evidence supporting the hypothesis that diatoms are the major nitrate-storing organisms in phototrophic microbial communities worldwide: (i) the highly significant correlation of total $ICNO_3$ contents with diatom abundance and biovolume (and also with fucoxanthin contents) across all habitat types, and (ii) the spatial and temporal co-occurrence of $ICNO_3$ and fucoxanthin maxima. This fits well with the previously demonstrated high $ICNO_3$ storage capacity of diatom isolates[8,12,24–27]. Since fucoxanthin is also found in microalgal classes other than diatoms and since total $ICNO_3$ contents correlated also with chlorophyll *a* contents, the potential contribution of other microalgal classes to total $ICNO_3$ contents was evaluated. Generally, the contribution of nitrate-storing microorganisms to total $ICNO_3$ contents in the environment increases with the $ICNO_3$ concentration level inside the cell, with cell volume, and with cell abundance. Among microalgae, diatoms store the by far highest $ICNO_3$ concentration levels and possess on average very large cells, which together results in cell-specific $ICNO_3$ contents that are typically two orders of magnitude higher than in any other microalgal class (Table 1). Even large-celled Dinophyceae would have to be ~100 times more abundant than diatoms to contribute the same amount of nitrate to the total $ICNO_3$ contents in a given habitat. However, the peridinin/chlorophyll *a* ratio (a proxy for the relative abundance of Dinophyceae) was on average >7 times lower in environmental samples than in Dinophyceae isolates (Supplementary Table 5). Additionally, the peridinin/chlorophyll *a* ratio did not correlate with total $ICNO_3$ contents across all habitat types (Supplementary Table 5). Taken together, it is very unlikely that Dinophyceae contributed substantially to total $ICNO_3$ contents in this survey. The same reasoning applies to Cryptophyceae, Chlorophyceae, cyanobacteria, and the extremely small Pelagophyceae. The pigment-based argumentation is less clear for Prymnesiophyceae and Chrysophyceae as they do not contain unequivocal marker pigments, but their very low $ICNO_3$ storage capacity still disqualifies them as important contributors to total $ICNO_3$ contents. Noteworthy, both fucoxanthin/chlorophyll *a* and diadinoxanthin/chlorophyll *a* ratios were nearly the same in environmental samples vs. diatom isolates, which argues for generally high relative diatom abundances in this survey.

Clearly, the most important determinant for the measured total $ICNO_3$ contents is habitat type. The connection between total $ICNO_3$ contents and habitat type must be mediated by the vastly differing diatom abundance and biovolume in phototrophic microbial communities of different aquatic habitats, which culminates in extremely high values of diatom abundance and biovolume and total $ICNO_3$ contents in epilithic biofilms. Additionally, the habitat types differed significantly in diatom community composition, with the exception of sediments and diatom mats. The latter observation is likely explained by the fact that diatom mats had developed on top of sediments and thus

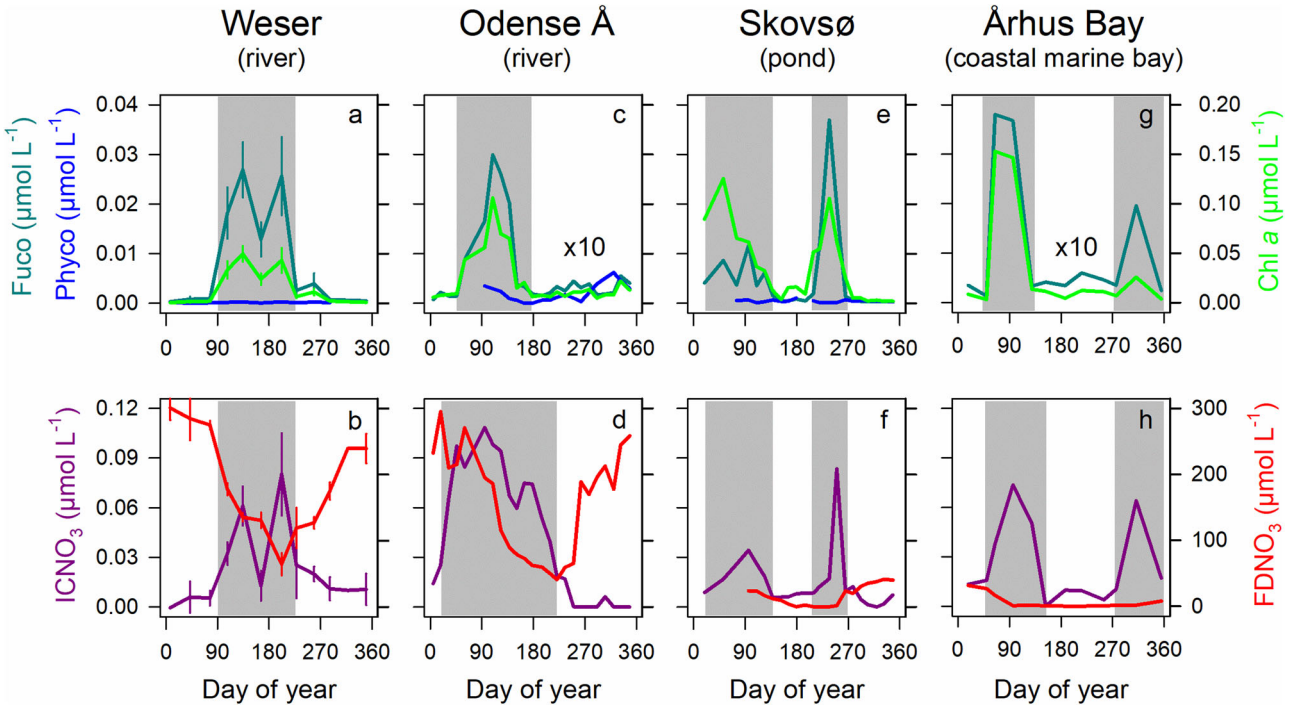

Fig. 5 Seasonal variation of intracellular nitrate. a, **c**, **e**, **g** Water column contents of chlorophyll *a* (Chl *a*), fucoxanthin (Fuco), and phycocyanin (Phyco) and **b**, **d**, **f**, **h** freely dissolved nitrate ($FDNO_3$) and intracellular nitrate ($ICNO_3$) in two rivers, one pond, and one coastal marine bay. For better visibility, photopigment and nitrate contents were multiplied by an appropriate factor as indicated in the respective panel. Gray shading marks time periods during which fucoxanthin and $ICNO_3$ maxima appeared. For Århus Bay, no phycocyanin data are available. For Weser, monthly means ± standard deviation of $n = 5$ were calculated from multiple samplings during 2017–2021.

diatom communities of the two habitat types may overlap. Different diatom species may possess different $ICNO_3$ storage capacities, as also observed for foraminifers[31], which may scale up to differences in total $ICNO_3$ contents in the environment. However, diatom community composition was not a significant determinant of total $ICNO_3$ contents in phototrophic microbial communities. This suggests that the ability to store $ICNO_3$ is widespread in diatoms and/or that species-specific differences in $ICNO_3$ storage capacity are averaged out in the highly diverse diatom communities.

Implications of $ICNO_3$ storage for diatoms. For the individual diatom cell, $ICNO_3$ serves as a buffer for time periods during which the cell is cut off from ambient $FDNO_3$ supply. This may be the case in environments where $FDNO_3$ is spatially constrained as in stratified water columns or benthic habitats[17,19], or where $FDNO_3$ concentrations fluctuate over time, such as in tidally flushed sediments[32,33]. For marine pelagic diatoms, the $ICNO_3$ pool is reported to last for 3–4 days[24,34], which is sufficient time for migrating between the nitrate-replete subsurface layer and the nitrate-depleted surface layer in the ocean[17]. For benthic diatoms, however, the $ICNO_3$ pool is reported to last for ~12–24 h only[12,19,33], which is still sufficient time for bridging nitrate-depleted conditions encountered during tidal cycles or migration in sediments or mats with steep concentration gradients[19,33]. The longer lifetime of the $ICNO_3$ pool in pelagic diatoms is consistent with the higher $ICNO_3$ concentrations inside the cells of pelagic diatoms documented in our survey.

Diatoms can use their $ICNO_3$ pool for N-assimilation[24,35]. In the size range of diatom cells in our survey (i.e., 550–19450 µm^3 per cell), the $ICNO_3$ pool of a single cell corresponded to ~1% of its total nitrogen content as estimated from cell volume[36]. This low value is consistent with another survey of different marine phytoplankton species[24] and implies that diatoms in this size range cannot sustain N-assimilation with their relatively small $ICNO_3$ pool alone, but must rely on intracellular ammonium, urea, and/or amino acids as additional nitrogen sources[24,37]. In contrast, in the very large pelagic diatom *Ethmodiscus* sp. (i.e., 5×10^8 µm^3 per cell), the $ICNO_3$ pool corresponds to 135% of the particulate organic nitrogen content and can support one cell division within four days[34]. This discrepancy is explained by the increase in relative vacuole volume with increasing cell size (i.e., from 30–60% for the size range of diatoms in our survey to >90% for *Ethmodiscus* sp. as estimated from cell volume[38]).

Diatoms possess an exceptional potential to survive dark and anoxic conditions through physiological and metabolic adaptations, such as DNRA activity, dark fermentation, and resting stage formation[12,39,40]. Diatom-mediated DNRA activity, in particular, is induced by a change from oxic to anoxic conditions due to, e.g., tidal-induced porewater movement, diatom migration behavior in benthic habitats, or passive sinking of diatom aggregates through an oxygen minimum zone[12,18,26]. The $ICNO_3$ pool can then be used for energy conservation through anaerobic nitrate respiration until oxic conditions re-establish within 12–24 h[12,19,33]. In cases where anoxic conditions persist for very long time periods (e.g., after settlement of diatoms onto anoxic sediments), diatoms might use the energy conserved through DNRA activity for the transition to a resting stage, which can be completed within 8–10 h[12,41].

Surprisingly, $ICNO_3$ storage was also observed in habitats in which neither $FDNO_3$ limitation, nor anoxic conditions are likely to occur, such as in the water column of nitrate-rich streams. One possible explanation for this phenomenon is that the cytosolic nitrate reductase of diatoms has a relatively low affinity (i.e., a high k_m value) for nitrate, which requires an intracellular up-concentration to enable high enzymatic conversion rates. Indeed, the k_m value of assimilatory nitrate reduction is 50–290 µmol L^{-1} and thus higher than $FDNO_3$ concentrations in many aquatic

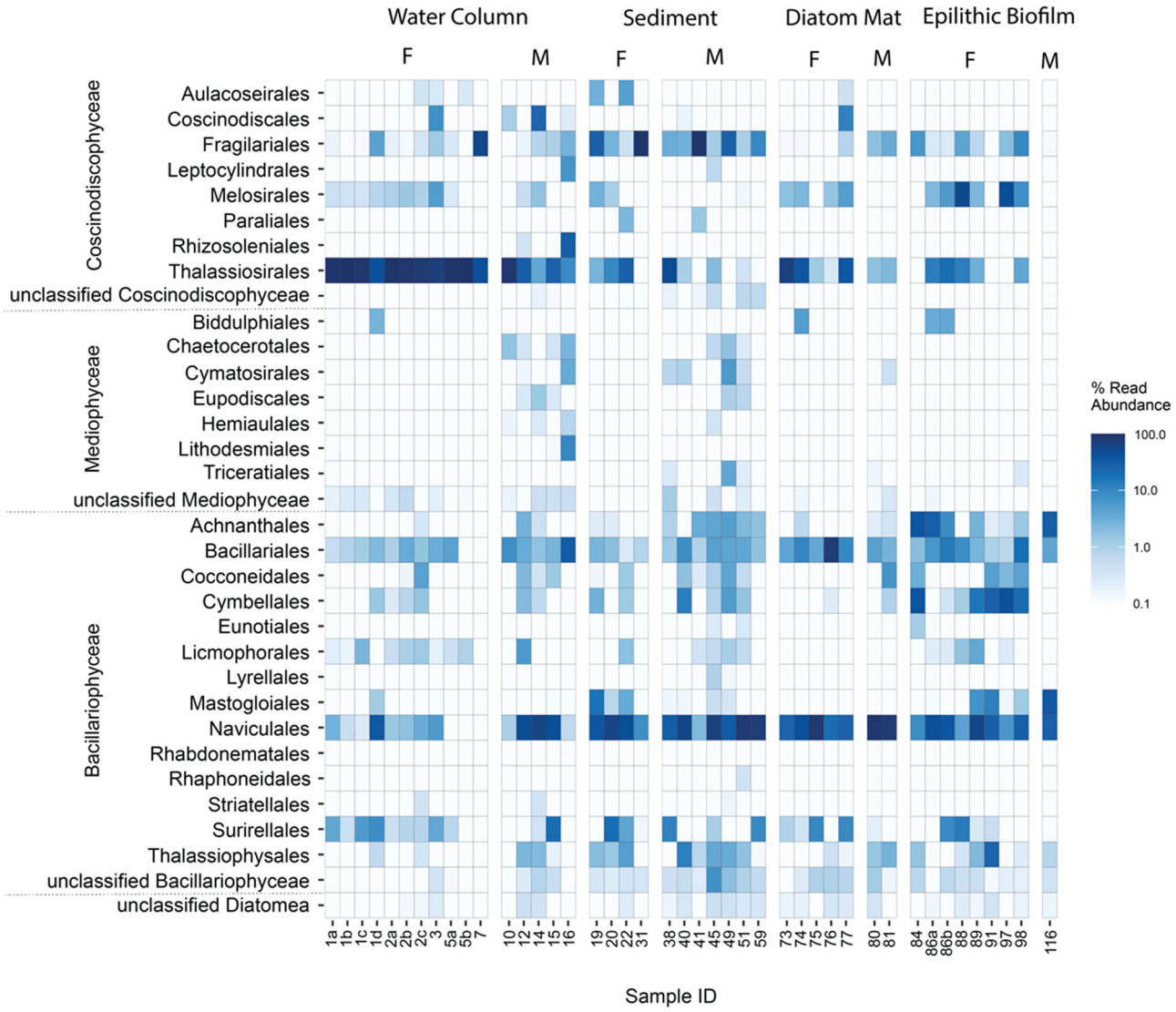

Fig. 6 Diatom community analysis. Heatmap of relative 18S rRNA gene sequence abundance at the level of diatom classes and orders for freshwater (F) and marine (M) water column, sediment, diatom mat, and epilithic biofilm samples. Relative sequence abundance scales from white (<0.15%) to dark blue (100%). Sample IDs are given in Supplementary Tab. 1 (Supplementary Data 1).

habitats[8]. Additionally, in diatoms exposed to rapidly increasing irradiance levels, $ICNO_3$ may be used for NRphot, the dissipation of excess photosynthetic energy via nitrate reduction to nitrite and/or ammonium, which are expelled from the cells[8,28–30]. The NRphot pathway has originally been described for pelagic diatom communities in the oceans, but might also exist in the nitrate-rich streams studied here where diatoms have unlimited access to nitrate, but experience pronounced differences in light levels due to the turbulent water flow. The NRphot pathway may also be of importance in microbial/diatom mats exposed to high irradiation levels, but this remains to be studied. Taken together, nitrate accumulation might be an evolved trait of diatoms that is constitutively expressed despite ample availability of $FDNO_3$.

Implications of $ICNO_3$ storage by diatoms for nitrogen cycling. The total $ICNO_3$ contents measured within a given aquatic habitat can be used to predict the occurrence of specific nitrate-fueled metabolic pathways, if the major nitrate-storing organisms are also known. For example, denitrification and DNRA are likely to occur in oxygen-depleted aquatic habitats in which foraminifers and diatoms, respectively, are abundant[11,12]. In the phototrophic microbial communities studied here, diatoms were the major nitrate-storing organisms and thus diatom-mediated N-assimilation, NRphot, and DNRA were likely the most important pathways fueled by $ICNO_3$. Utilizing either pathway, diatoms contribute to the retention of fixed nitrogen in the ecosystem in the form of (particulate) organic nitrogen, ammonium, and/or nitrite rather than to the loss of fixed nitrogen to dinitrogen gas as occurs through denitrification and anammox[1].

Beyond this qualitative assessment, it is not possible to predict the quantitative extent to which nitrogen cycling is impacted by nitrate-storing diatoms as only the size of the $ICNO_3$ pool was measured but not its turnover. Pure culture studies indicate that the $ICNO_3$ pool of diatoms is turned over on time scales of minutes to hours through NRphot[28–30] and DNRA[12,25]. The very few studies on nitrate-storing diatoms in environmental settings report turnover times of the $ICNO_3$ pool on the order of hours to days[19,26,33]. Ultimately, the rates of nitrogen-cycle pathways fueled by $ICNO_3$ vs. $FDNO_3$ will have to be compared in situ to gauge the contribution by nitrate-storing diatoms to nitrogen cycling, a task that is still pending.

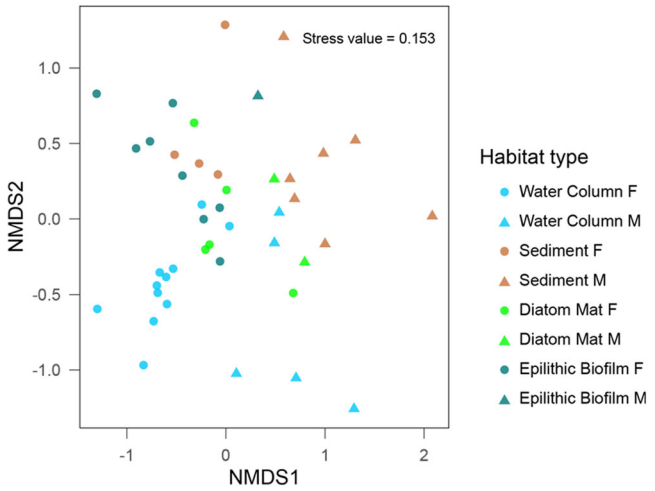

Fig. 7 Diatom community analysis. NMDS plot of Bray–Curtis dissimilarities from 43 diatom communities with a total of 2157 amplicon sequence variants (ASVs) retrieved from different habitat types.

In the pelagic zone of nutrient-rich freshwater and marine ecosystems, total $ICNO_3$ contents are usually in the nanomolar range and contribute <1% to total nitrate, even during diatom blooms[42–44,this survey]. In oligotrophic regions of the open ocean, which are not represented in our dataset, the relative contribution of $ICNO_3$ to total nitrate remains unresolved. However, at nitrate concentrations of ~10 nmol L^{-1} in the surface water of these regions, only one single cell of *Ethmodiscus* sp., which stores 11 nmol $ICNO_3$, needs to be present in 1 L seawater to reach a relative contribution of ~50%[34]. Additionally, NRphot activity by pelagic diatoms may be significant due to turbulent water flow, for example, in coastal upwelling zones of the oceans where diatoms are abundant[8,21,28]. Since $ICNO_3$ is turned over to and expelled as nitrite and/or ammonium, NRphot activity by pelagic diatoms supplies nitrifying microorganisms with substrates, a link not established in situ so far. High NRphot activity represents also a methodological issue because it is assumed to bias "new production" estimates for the oceans[29]. DNRA activity by pelagic diatoms is likely precluded by the presence of oxygen in most water columns, but occurs inside anoxic "marine snow" aggregates that display DNRA rates equivalent to 16–28% of denitrification rates[26,45]. However, even at high aggregate abundance in the water column of oxygen minimum zones, these DNRA rates are low (<1 nmol NH_4^+ L^{-1} d^{-1} (ref. [45]) relative to DNRA rates in the ambient water of up to 40 nmol NH_4^+ L^{-1} d^{-1} (ref. [46]).

In benthic habitats with abundant diatoms, $ICNO_3$-fueled DNRA rates may indeed rival $FDNO_3$-fueled denitrification rates. In an intertidal sediment, the $ICNO_3$ stored by the diatom-dominated eukaryotic community fueled DNRA activity equivalent to ~10–20% of denitrification activity[3,33]. In a mat-covered lake sediment, DNRA activity made up 98–99% of total dissimilatory nitrate reduction and was ascribed to the nitrate-storing and migrating diatom *Craticula cuspidata*[19]. Notably, this dominance of DNRA coincided with an extremely high relative contribution of $ICNO_3$ to total nitrate of 98%. In a rocky biofilm, high DNRA activity corresponding to 59–69% of total dissimilatory nitrate reduction and was ascribed to anoxic conditions prevailing at night[47]. While the presence of diatoms in this rocky biofilm was not reported, essentially all epilithic biofilms studied in our survey were dominated by nitrate-storing diatoms and might thus emerge as hotspots of NRphot activity during the day and DNRA activity at night. Notably, these reported relative contributions of $ICNO_3$ turnover by diatoms to benthic nitrogen cycling are in a similar range as the relative contribution of $ICNO_3$ contents to total nitrate contents as established in our survey for benthic habitats (i.e., 65–95%). The reason why diatom-mediated DNRA activity, in particular, might have been overlooked so far pertains to the general neglect of DNRA compared to denitrification and anammox in N-cycle studies[3,48] and the common perception that phototrophic communities do not host anaerobic nitrogen cycling because of photosynthetic oxygen production during daytime. However, phototrophic sediments and mats are always underlain by anoxic subsurface layers and even thin phototrophic biofilms may experience anoxia in darkness due to high community respiration rates[49,50]. Also very large aggregations of pelagic diatoms, such as the centimeter- to meter-scale strands of *Melosira arctica* underneath sea-ice floes[51,52], might emerge as oxygen-depleted microenvironments in which $ICNO_3$ storage and DNRA activity occur. The widespread occurrence of $ICNO_3$ storage by diatoms demonstrated in this survey and the growing number of diatom isolates capable of DNRA strongly suggest that significant DNRA activity will be discovered in many more aquatic ecosystems.

Methods

Sample collection and preparation. Phototrophic microbial communities were sampled across diverse freshwater and marine ecosystems on all continents and in all climate zones (Fig. 1, Supplementary Table 1, Supplementary Data 1). The sampling sites covered four different habitat types: water column, sediment, microbial mat, and epilithic biofilm. Vertical profiles of intracellular nitrate ($ICNO_3$) contents were recorded in the water column, sediment, and microbial mat of 16 sampling sites. Seasonal cycles of $ICNO_3$ contents were monitored in the water column of four sampling sites. Snapshot samples were collected at 117 globally distributed sampling sites.

Water column samples were collected using (i) 2-L polyethylene bottles for surface water samples and (ii) 8-L Niskin bottles for deeper water samples. Water volumes of 0.1–2 L were filtered through pre-combusted 0.3-µm glass fiber filters (GF75, Advantec Inc., U.S.A.) that were stored in 15-mL sample tubes at −20 °C for later analysis of $ICNO_3$ and photopigments. An aliquot of 1 mL filtrate was stored at −20 °C for later analysis of freely dissolved nitrate ($FDNO_3$).

Sediment samples were collected using (i) perspex core liners (3.6 cm internal diameter) to retrieve ~15-cm-long sediment cores or (ii) weighing spoons to scoop the top 0.5 or 1 cm of sediment into 50-mL sample tubes that were 1/3 filled with sediment, 1/3 overlying water (to maintain nitrate availability), and 1/3 air (to maintain oxic conditions). Sediment samples were processed in the laboratory within 1–2 h after collection (sediment cores) or 1–7 days after collection and transport (sediment top layers). Intact sediment cores were sliced at 0.5-1-cm intervals to a total depth of 5–10 cm. Each slice of known wet volume was split into three equal parts and transferred to 15-mL sample tubes for later analysis of nitrate as well as lysozyme- and acetone/ethanol-extracted photopigments. Sediment top layers were vigorously mixed, split into three equal parts, and transferred to 15-mL sample tubes for nitrate and photopigment analyses. The split samples were mildly centrifuged (500 × *g* for 5 min) to determine the individual wet volume as read from the scale of the sample tube.

Microbial mats were collected as (i) ~10 mm-thick laminated mats that were retrieved using a scalpel and (ii) ~1 mm-thin "diatom mats" that were skimmed off sediment surfaces using a weighing spoon. Laminated mats were originally sampled in the field and maintained in the laboratory under in situ conditions regarding light regime, temperature, and salinity for longer time periods[53,54]. Mat samples were processed in the laboratory immediately after harvesting them from maintenance tanks (laminated mats) or within 1 h after collection at the sampling site (diatom mats). Laminated mats were sliced using a stainless steel tube (1 cm internal diameter) for coring and a stainless steel rod (1 cm outer diameter) and a spatula for extruding and slicing the mat core, respectively. The thickness of the mat slices was guided by the visible functional layering of each mat. For mats with unclear functional layering, the top 1 cm was treated as one bulk sample. Diatom mat samples were treated in the same way as sediment top layers.

Epilithic biofilms were collected as intact biofilms covering (i) pebbles that were transported in 50-mL sample tubes or (ii) larger stones that were transported in 250-mL plastic containers. Samples were processed in the laboratory within 1–2 h after collection (local sites) or 1–7 days after collection and transport (remote sites). Biofilms were detached from pebbles and larger stones by abrasion and brushing, respectively. All pebbles from one 50-mL sample tube were transferred to a 250-mL polyethylene bottle to which 50 mL of nitrate-free water (NFW) prepared from Red Sea salt (Red Sea Aquatics Ltd., U.K.) was added. For freshwater and marine samples, NFW was prepared at salinities of 0.02 and 35, respectively, and adjusted to pH values of 7.0 and 8.2, respectively. The closed bottle was vigorously shaken

for 2 min to enable abrasion of biofilms as the pebbles rubbed against each other. The obtained biofilm suspension was split into three equal parts and transferred into 15-mL sample tubes for $ICNO_3$ and photopigment analyses. The first round of centrifugation at 500 × *g* for 5 min served to determine the wet volume of the biofilm. The second round of centrifugation at 3000 × *g* for 5 min served to compact the biofilm pellet so that the clear supernatant could be discarded. Biofilms on larger stones (up to 10 cm in diameter) were thoroughly brushed off using a vegetable brush and with the stone submerged in 100 mL of NFW. The obtained biofilm suspension was processed as described for pebble samples.

Microalgal isolates were screened for their $ICNO_3$ storage capacity in laboratory incubations. Twenty isolates from five microalgal classes for which published $ICNO_3$ data were not available or very sparse and six diatom isolates were studied (Supplementary Table 4 and Supplementary Data 4). The microalgal isolates were grown in F/2 or L1 media in a light:dark cycle of 16:8 h and at 4 or 15 °C. For $ICNO_3$ determination, 20 mL of cell suspension of each isolate was centrifuged at 500 × *g* for 10 min, the spent growth media potentially still containing nitrate discarded, and the cell pellet resuspended in 20 mL 0.2-µm-filtered NFW amended with 25 µmol L^{-1} $NaNO_3$. The cell suspension was equally distributed between four transparent 15-mL sample tubes, incubated for a full light:dark cycle of 16:8 h, and harvested at 9 a.m. local time, which was 3 h after the start of the light period. The cell suspensions were thoroughly mixed and a 1-mL subsample was taken and fixed with formaldehyde (1% final concentration) for later cell counting and cell volume determination. The remaining sample volume was used for $ICNO_3$ determination and pigment analysis.

Intracellular nitrate determination. For $ICNO_3$ extraction from water column samples, 5 mL of deionized water was added to the filter in the sample tube before it was snap-frozen in liquid nitrogen. To further promote the destruction of microbial cells on the filter, the tube was transferred to a water bath kept at 80–90 °C until the sample was completely thawed. This freeze-thaw cycle was repeated a second time[55]. The extracted sample was centrifuged at 3000 × *g* for 5 min and 1 mL of the supernatant was stored at −20 °C for later analysis.

For $ICNO_3$ and porewater nitrate ($PWNO_3$) extraction from sediment, mat, and biofilm samples, 3 mL of NFW was added to the sample, vigorously mixed, and centrifuged at 3000 × *g* for 5 min. From the clear supernatant, 1 mL was stored at −20 °C for later $PWNO_3$ analysis. From the remaining sample, $ICNO_3$ was extracted by freeze-thaw cycling.

For $ICNO_3$ extraction from microalgal isolates, the cell suspensions in three replicate tubes were centrifuged at 500 × *g* for 10 min and 1 mL of the supernatant was taken for $FDNO_3$ analysis. From the remaining sample, $ICNO_3$ was extracted by freeze-thaw cycling. The $ICNO_3$ concentration inside microalgal cells was calculated from the difference between $ICNO_3$ and $FDNO_3$ concentrations, the cell abundance, and the cell volume of the respective microalgal isolate.Nitrate concentrations were measured spectrophotometrically using the protocol by[56]. This two-step reaction assay combines the Griess reaction for nitrite determination[57] and the VCl_3 reduction method for NO_x (i.e., nitrate plus nitrite) determination[58]. Since nitrite concentrations were generally negligible, NO_x concentrations are reported here as nitrate concentrations.

Total $ICNO_3$ contents of water column samples were calculated from the nitrate concentration in the filter extract corrected for $FDNO_3$ in the water-soaked filter and the volume of filtered water. Total $ICNO_3$ contents of sediment, mat, and biofilm samples were calculated as the difference in nitrate contents before ($PWNO_3$) and after the extraction step ($PWNO_3 + ICNO_3$).

The relative contribution of $ICNO_3$ to total nitrate in each sample was calculated as $ICNO_3/(ICNO_3 + FDNO_3)$ for water column samples and as $ICNO_3/(ICNO_3 + PWNO_3)$ for sediment, mat, and biofilm samples and expressed in percent.

Photopigment determination. Photopigments were extracted by adding 5 mL of ice-cold, HPLC-grade acetone:ethanol (1:1) to the sample and keeping it at −20 °C for 24 h during which it was repeatedly shaken by hand. The extracted sample was centrifuged at 3000 × *g* for 5 min and 1.5 mL of the supernatant was filtered through a 0.45 µm Versapor® membrane (Acrodisc®, Gelman Laboratory) into 2-mL glass vials with a septum cap. Samples were kept in darkness and on ice during extraction and filtration. The extracted pigments were separated and analyzed on a Waters UPLC H-Class system (Waters, Milford, USA) equipped with an Acquity UPLC BEH C18 column (1.7 µm, 2.1 × 150 mm) (Waters, Milford, USA). Solvent gradients, column temperature, and flow rate were as described in ref. [59]. In the chromatograms, ten different photopigments were identified according to their specific retention time and absorption spectra and the respective peaks were integrated. Calibrations were made with serially diluted stock solutions of the respective photopigment (DHI, Denmark).

The water-soluble photopigment phycocyanin (a cyanobacteria marker pigment) was extracted by adding 5 mL of lysozyme (15 g L^{-1} in 65 mM phosphate buffer adjusted to pH 8.2) to the sample and keeping it at 37 °C for 2 h during which it was repeatedly shaken by hand. The lysed sample was centrifuged at 3000 × *g* for 5 min and 1.5 mL of the clear supernatant was transferred into a 2-mL microcuvette and analyzed spectrophotometrically according to[60]. The obtained phycocyanin concentrations in g L^{-1} were recalculated to molar concentrations using the molar mass of phycocyanin of 30 kg mol^{-1} [61].

Diatom abundance and biovolume. For a subset of 6–8 samples from each habitat type and three replicates each, diatom cells were counted and sized by microscopy. Samples were fixed in formaldehyde (1% final concentration) at 4 °C for 24 h. The fixed samples were diluted 100–2000× with 0.2-µm-filtered NFW and vigorously mixed for 2 min. Aliquots of the resulting cell suspension were used for cell counting in a Fuchs-Rosenthal chamber by phase-contrast microscopy[12]. For each sample and replicate, 140–570 diatom cells were counted, and the cell numbers obtained were recalculated to diatom abundance per unit volume of sample. For biovolume determination, 10–20 light micrographs were taken for each sample and replicate. Length and width of 100–200 individual cells per sample were measured with the image-processing program ImageJ (W.S. Rasband, NIH, Bethesda, U.S.A.). The cell volume of different diatom morphotypes was approximated using equations for different geometric shapes[62]. The total diatom biovolume per unit volume of sample was calculated from the diatom abundance and the average cell volume determined for each sample.

Diatom community composition

DNA extraction and PCR. For a selected subset of 53 samples representing all habitat types, the diatom community composition was analyzed by 18S rRNA gene sequencing. Water column samples (0.25–1 L) were filtered through 0.22-µm nylon membrane filters (Montamil®, Frisenette ApS, Denmark), from which DNA was extracted using the Allprep DNA/RNA Minikit (Qiagen No. 80204, Germany). The DNA of sediment, mat, and biofilm samples (0.05–5 mL) was extracted using the DNeasy PowerLyzer PowerSoil Kit (Qiagen No. 12855, Germany).

Three rounds of PCR were used to prepare the samples for 18S rRNA gene sequencing; first, the 18S rRNA gene was amplified using the diatom-targeted primer pair D512F/D978R[63]. The amplification was run in 25 µL reactions containing 2 µL template DNA, 12.5 µL 2X KAPA HiFi Hotstart Readymix (KAPA Biosystems), 0.5 µL bovine serum albumin (10 mg mL^{-1}), 9 µL dH_2O and 0.5 µL of each primer (10 pmol $µL^{-1}$). Cycling conditions were: 95 °C for 3 min, followed by 35 cycles of 95 °C for 45 s, 55 °C for 30 s and 72 °C for 20 s, with a final elongation at 72 °C for 5 min. In the second round of PCR, Illumina adapters were added by using primers carrying the forward and reverse adapter overhang sequences at their 5' ends. The adapter sequence information is provided in Illumina's 16S metagenomic sequencing library preparation protocol (Illumina). The reaction conditions consisted of 12.5 µL KAPA HiFi Hotstart Readymix, 2.5 µL of purified PCR product, and 0.5 µL of each primer. Cycling conditions were: 95 °C for 3 min, 10 cycles of 95 °C for 30 s, 55 °C for 30 s, and 72 °C for 30 s, with a final elongation at 72 °C for 5 min. The PCR products from the second PCR were purified with the Agencourt AMPure XP PCR Purification system (Beckman Coulter). Subsequently, indices were added in the third round of PCR using the same conditions as the second PCR, except with only 8 PCR cycles. Products were purified with AMPure XP beads and paired-end sequenced in 2 × 301 cycles on an Illumina MiSeq Desktop sequencer using the MiSeq v3 Reagent Kit according to standard protocols. Samples were sequenced in two separate MiSeq runs.

18S rRNA gene sequence analysis. All analyses were run in R version 4.04. Trimming of adapter and PCR primers were done with cutadapt v0.1.1[64]. The R package "dada2" v. 1.18.0[65] was used for sequence filtering, denoising, paired-end merging and taxonomic classification. Samples from the two MiSeq runs were filtered and denoised separately to obtain an individual error model for each run with the DADA algorithm. After denoising, the two MiSeq runs were merged for detecting and removing chimeras. Finally, the amplicon sequence variants (ASVs) were taxonomically assigned using the Silva SSU reference database no. 138[66]. For ASVs with a relative abundance >0.15%, the taxonomic assignment was manually corrected at order and class level according to the taxonomies presented in refs. [67,68], respectively, performing BLAST and Taxonomy Browser searches (NCBI). Four ASVs that were predominantly found in negative PCR controls, but only in low abundance in actual samples, were removed from subsequent analyses.

Statistical analysis. Spearman's rank correlation coefficients were calculated for monotonic relationships between two variables. To test whether the correlation coefficients were significantly different from zero, two-sided Student's *t*-tests with $n - 2$ degrees of freedom were used. Community analysis of the classified ASVs was done using the R packages phyloseq v1.34.0[69] and ampvis2 v2.6.5, and all plots were made with ggplot2 v3.3.3[70]. We used vegan v2.5.7[71] for calculating analysis of similarity (ANOSIM) and permutational multivariate analysis of variance (PERMANOVA) tests.

Reporting summary. Further information on research design is available in the Nature Research Reporting Summary linked to this article.

Data availability

The source data for Figs. 2–5 have been deposited at figshare (https://doi.org/10.6084/m9.figshare.19790176.v1)[72]. The sequence data for Figs. 6, 7 have been deposited at NCBI GenBank under Biosample accession numbers from SAMN23488989 to SAMN23489046.

Received: 6 February 2022; Accepted: 21 June 2022;
Published online: 04 July 2022

References

1. Thamdrup, B. New Pathways and processes in the global nitrogen cycle. *Annu. Rev. Ecol. Evol. Syst.* **43**, 407–428 (2012).
2. Lam, P. et al. Revising the nitrogen cycle in the Peruvian oxygen minimum zone. *Proc. Natl. Acad. Sci. USA* **106**, 4752–4757 (2009).
3. Behrendt, A., de Beer, D. & Stief, P. Vertical activity distribution of dissimilatory nitrate reduction in coastal marine sediments. *Biogeosciences* **10**, 7509–7523 (2013).
4. Fossing, H. et al. Concentration and transport of nitrate by the mat-forming sulphur bacterium. *Thioploca. Nature* **374**, 713–715 (1995).
5. McHatton, S. C., Barry, J. P., Jannasch, H. W. & Nelson, D. C. High nitrate concentrations in vacuolate, autotrophic marine *Beggiatoa* spp. *Appl. Environ. Microbiol.* **62**, 954–958 (1996).
6. Kamp, A., Høgslund, S., Risgaard-Petersen, N. & Stief, P. Nitrate storage and dissimilatory nitrate reduction by eukaryotic microbes. *Front. Microbiol.* **6**, 1492 (2015).
7. Eppley, R. W. & Rogers, J. N. Inorganic nitrogen assimilation of *Ditylum brightwellii*, a marine plankton diatom. *J. Phycol.* **6**, 344–351 (1970).
8. Lomas, M. & Glibert, P. Comparisons of nitrate uptake, storage, and reduction in marine diatoms and flagellates. *J. Phycol.* **36**, 903–913 (2000).
9. Jørgensen, B. B. & Gallardo, A. *Thioploca* spp.: filamentous sulfur bacteria with nitrate vacuoles. *FEMS Microbiol. Ecol.* **28**, 301–313 (1999).
10. Schulz, H. N. et al. Dense populations of a giant sulfur bacterium in Namibian shelf sediments. *Science* **284**, 493–495 (1999).
11. Risgaard-Petersen, N. et al. Evidence for complete denitrification in a benthic foraminifer. *Nature* **443**, 93–96 (2006).
12. Kamp, A., de Beer, D., Nitsch, J. L., Lavik, G. & Stief, P. Diatoms respire nitrate to survive dark and anoxic conditions. *Proc. Natl. Acad. Sci. USA* **108**, 5649–5654 (2011).
13. Stief, P. et al. Dissimilatory nitrate reduction by *Aspergillus terreus* isolated from the seasonal oxygen minimum zone in the Arabian Sea. *BMC Microbiol.* **14**, 35 (2014).
14. Høgslund, S., Cedhagen, T., Bowser, S. S. & Risgaard-Petersen, N. Sinks and sources of intracellular nitrate in gromiids. *Front. Microbiol.* **8**, 617 (2017).
15. Harold, F. M. *The Vital Force: A Study of Bioenergetics* (WH Freeman & Co., 1986).
16. Katz, M. E., Finkel, Z. V., Grzebyk, D., Knoll, A. H. & Falkowski, P. G. Evolutionary trajectories and biogeochemical impacts of marine eukaryotic phytoplankton. *Annu. Rev. Ecol. Evol. Syst.* **35**, 523–556 (2004).
17. Villareal, T. A., Altabet, M. A. & Culverrymsza, K. Nitrogen transport by vertically migrating diatom mats in the North Pacific Ocean. *Nature* **363**, 709–712 (1993).
18. Kamp, A., Stief, P. & Schulz, H. N. Anaerobic sulfide oxidation with nitrate by a freshwater *Beggiatoa* enrichment culture. *Appl. Environ. Microbiol.* **72**, 4755–4760 (2006).
19. Merz, E. et al. Nitrate respiration and diel migration patterns of diatoms are linked in sediments underneath a microbial mat. *Environ. Microbiol.* **23**, 1422–1435 (2021).
20. Leblanc, K. et al. A global diatom database–abundance, biovolume and biomass in the world ocean. *Earth Syst. Sci. Data* **4**, 149–165 (2012).
21. Benoiston, A. S. et al. The evolution of diatoms and their biogeochemical functions. *Phil. Trans. R. Soc. B* **372**, 20160397 (2017).
22. Nelson, D. M., Tréguer, P., Brzezinski, M. A., Leynaert, A. & Queguiner, B. Production and dissolution of biogenic silica in the ocean-revised global estimates, comparison with regional data and relationship to biogenic sedimentation. *Global Biogeochem. Cycl.* **9**, 359–372 (1995).
23. Sarthou, G., Timmermans, K. R., Blain, S. & Tréguer, P. Growth physiology and fate of diatoms in the ocean: a review. *J. Sea Res.* **53**, 25–42 (2005).
24. Dortch, Q., Clayton, J. R., Thoresen, S. S. & Ahmed, S. I. Species differences in accumulation of nitrogen pools in phytoplankton. *Mar. Biol.* **81**, 237–250 (1984).
25. Kamp, A., Stief, P., Knappe, J. & de Beer, D. Response of the ubiquitous pelagic diatom *Thalassiosira weissflogii* to darkness and anoxia. *PLoS ONE* **8**, e82605 (2013).
26. Kamp, A., Stief, P., Bristow, L. A., Thamdrup, B. & Glud, R. N. Intracellular nitrate of marine diatoms as a driver of anaerobic nitrogen cycling in sinking aggregates. *Front. Microbiol.* **7**, 1669 (2016).
27. Needoba, J. A. & Harrison, P. J. Influence of low light and a light:dark cycle on NO_3^- uptake, intracellular NO_3^-, and nitrogen isotope fractionation by marine phytoplankton. *J. Phycol.* **40**, 505–516 (2004).
28. Lomas, M. W. & Glibert, P. M. Temperature regulation of nitrate uptake: A novel hypothesis about nitrate uptake and reduction in cool-water diatoms. *Limnol. Oceanogr.* **44**, 556–572 (1999).
29. Lomas, M. W., Rumbley, C. J. & Glibert, P. M. Ammonium release by nitrogen sufficient diatoms in response to rapid increases in irradiance. *J. Plankton Res.* **22**, 2351–2366 (2000).
30. Van Tol, H. M. & Armbrust, E. V. Genome-scale metabolic model of the diatom *Thalassiosira pseudonana* highlights the importance of nitrogen and sulfur metabolism in redox balance. *PLoS ONE* **16**, e0241960 (2021).
31. Piña-Ochoa, E. et al. Widespread occurrence of nitrate storage and denitrification among Foraminifera and *Gromiida*. *Proc. Natl. Acad. Sci. USA* **107**, 1148–1153 (2010).
32. García-Robledo, E., Corzo, A., Papaspyrou, S., Jimenez-Arias, J. L. & Villahermosa, D. Freeze-lysable inorganic nutrients in intertidal sediments: dependence on microphytobenthos abundance. *Mar. Ecol. Prog. Ser.* **403**, 155–163 (2010).
33. Marchant, H. K., Lavik, G., Holtappels, M. & Kuypers, M. M. M. The fate of nitrate in intertidal permeable sediments. *PLoS ONE* **9**, e104517 (2014).
34. Villareal, T. A. & Lipschultz, F. Internal nitrate concentrations in single cells of large phytoplankton from the Sargasso Sea. *J. Phycol.* **31**, 689–696 (1995).
35. Smith, G. J., Zimmerman, R. C. & Alberte, R. S. Molecular and physiological responses of diatoms to variable levels of irradiance and nitrogen availability: Growth of *Skeletonema costatum* in simulated upwelling conditions. *Limnol. Oceanogr.* **37**, 989–1007 (1992).
36. Montagnes, D. J. S. & Franklin, D. J. Effect of temperature on diatom volume, growth rate, and carbon and nitrogen content: Reconsidering some paradigms. *Limnol. Oceanogr.* **46**, 2008–2018 (2001).
37. Smith, S. R. et al. Evolution and regulation of nitrogen flux through compartmentalized metabolic networks in a marine diatom. *Nat. Commun.* **10**, 4552 (2019).
38. Behrenfeld, M. J. et al. Thoughts on the evolution and ecological niche of diatoms. *Ecol. Monogr.* **91**, e01457 (2021).
39. Bourke, M. F. et al. Metabolism in anoxic permeable sediments is dominated by eukaryotic dark fermentation. *Nat. Geosci.* **10**, 30–35 (2017).
40. Härnström, K., Ellegaard, M., Andersen, T. J. & Godhe, A. Hundred years of genetic structure in a sediment revived diatom population. *Proc. Natl. Acad. Sci. USA* **108**, 4252–4257 (2011).
41. Pelusi, A., Santelia, M. E., Benvenuto, G., Godhe, A. & Montresor, M. The diatom *Chaetoceros socialis*: spore formation and preservation. *Europ. J. Phycol.* **55**, 1–10 (2020).
42. Petterson, K. & Sahlsten, E. Diel patterns of combined nitrogen uptake and intracellular storage of nitrate by phytoplankton in the open Skagerrak. *J. Exp. Mar. Biol. Ecol.* **138**, 167–182 (1990).
43. Petterson, K. Seasonal uptake of carbon and nitrogen and intracellular storage of nitrate in planktonic organisms in the Skagerrak. *J. Exp. Mar. Biol. Ecol.* **151**, 121–1137 (1991).
44. Bode, A., Botas, J. A. & Fernandez, E. Nitrate storage by phytoplankton in a coastal upwelling environment. *Mar. Biol.* **129**, 399–406 (1997).
45. Stief, P., Kamp, A., Thamdrup, B. & Glud, R. N. Anaerobic nitrogen turnover by sinking diatom aggregates at varying ambient oxygen levels. *Front. Microbiol.* **7**, 98 (2016).
46. Jensen, M. M. et al. Intensive nitrogen loss over the Omani Shelf due to anammox coupled with dissimilatory nitrite reduction to ammonium. *ISME J.* **5**, 1660–1670 (2011).
47. Magalhaes, C. M., Wiebe, W. J., Joye, S. B. & Bordalo, A. A. Inorganic nitrogen dynamics in intertidal rocky biofilms and sediments of the Douro River estuary (Portugal). *Estuaries* **28**, 592–607 (2005).
48. Burgin, A. J. & Hamilton, S. K. Have we overemphasized the role of denitrification in aquatic ecosystems? A review of nitrate removal pathways. *Front. Ecol. Environ.* **5**, 89–96 (2007).
49. Kühl, M., Glud, R. N., Ploug, H. & Ramsing, N. B. Microenvironmental control of photosynthesis and photosynthesis-coupled respiration in an epilithic cyanobacterial biofilm. *J. Phycol.* **32**, 799–812 (1996).
50. Heisterkamp, I. M. et al. Shell biofilm-associated nitrous oxide production in marine molluscs: processes, precursors and relative importance. *Environ. Microbiol.* **15**, 1943–1955 (2013).
51. Fernandez-Mendez, M. et al. Composition, buoyancy regulation and fate of ice algal aggregates in the Central Arctic Ocean. *PLoS ONE* **9**, e107452 (2014).
52. Boetius, A. et al. Export of algal biomass from the melting Arctic sea ice. *Science* **339**, 1430–1432 (2013).
53. Abed, R. M. M. & Garcia-Pichel, F. Long-term compositional changes after transplant in a microbial mat cyanobacterial community revealed using a polyphasic approach. *Environ. Microbiol.* **3**, 53–62 (2001).
54. Al-Najjar, M. A. A., de Beer, D., Kühl, M. & Polerecky, L. Light utilization efficiency in photosynthetic microbial mats. *Environ. Microbiol.* **14**, 982–992 (2012).

55. Heisterkamp, I. M., Kamp, A., Schramm, A. T., de Beer, D. & Stief, P. Indirect control of the intracellular nitrate pool of intertidal sediment by the polychaete *Hediste diversicolor*. *Mar. Ecol. Prog. Ser.* **445**, 181–192 (2012).
56. García-Robledo, E., Corzo, A. & Papaspyrou, S. A fast and direct spectrophotometric method for the sequential determination of nitrate and nitrite at low concentrations in small volumes. *Mar. Chem.* **162**, 30–36 (2014).
57. Grasshoff, K. In *Methods of Seawater Analysis* (eds Grasshoff, K., Ehrhardt, M., Kremling, K.) 143–150 (Verlag Chemie Weinheim, 1983).
58. Braman, R. S. & Hendrix, S. A. Nanogram nitrite and nitrate determination in environmental and biological materials by vanadium(III) reduction with chemiluminescence detection. *Anal. Chem.* **61**, 2715–2718 (1989).
59. Meier, D. V. et al. Limitation of microbial processes at saturation-level salinities in a microbial mat covering a coastal salt flat. *Appl. Environ. Microbiol.* **87**, e00698–21 (2021).
60. Sode, K., Horikoshi, K., Takeyama, H., Nakamura, N. & Matsunaga, T. Online monitoring or marine cyanobacterial cultivation based on phycocyanin fluorescence. *J. Biotechnol.* **21**, 209–217 (1991).
61. Berns, D. S., Scott, E. & Oreilly, K. T. C-phycocyanin-minimum molecular weight. *Science* **145**, 1054–1055 (1964).
62. Hillebrand, H., Durselen, C. D., Kirschtel, D., Pollingher, U. & Zohary, T. Biovolume calculation for pelagic and benthic microalgae. *J. Phycol.* **35**, 403–424 (1999).
63. Zimmermann, J., Jahn, R. & Gemeinholzer, B. Barcoding diatoms: evaluation of the V4 subregion on the 18S rRNA gene, including new primers and protocols. *Org. Divers. Evol.* **11**, 173–192 (2011).
64. Martin, M. Cutadapt removes adapter sequences from high-throughput sequencing reads. *EMBnet J.* **17**, 10–12 (2011).
65. Callahan, B. J. et al. DADA2: High-resolution sample inference from Illumina amplicon data. *Nat. Methods* **13**, 581–583 (2016).
66. Quast, C. et al. The SILVA ribosomal RNA gene database project: improved data processing and web-based tools. *Nucl. Acids Res.* **41**, D590–D596 (2013).
67. Round, F. E., Crawford, R. M. & Mann, D. G. *The Diatoms: Biology and Morphology of the Genera*. 747p (Cambridge University Press, 1990).
68. Medlin, L. K. Evolution of the diatoms: major steps in their evolution and a review of the supporting molecular and morphological evidence. *Phycologia* **55**, 79–103 (2016).
69. McMurdie, P. J. & Holmes, S. phyloseq: An R package for reproducible interactive analysis and graphics of microbiome census data. *PLoS ONE* **8**, e61217 (2013).
70. Wickham, H. *ggplot2: Elegant Graphics for Data Analysis* (Springer Verlag, 2016).
71. Oksanen, J. et al. *vegan: Community Ecology Package. R package version 2.5-7*. https://CRAN.R-project.org/package=vegan (2020).
72. Stief, P. *Intracellular Nitrate Storage by Diatoms-Source data. figshare. Dataset*. https://doi.org/10.6084/m9.figshare.19790176.v1 (2022).

Acknowledgements

This study was supported by grants from the German Science Foundation awarded to P.S. (STI 202/6) and A.K. (KA 3187/2-1), by the Max Planck Society (Germany), by the European Union's Seventh Framework Program for Research and Technological Development including Demonstration Activities awarded to Aarhus Institute of Advanced Studies (Grant agreement No. 609033), and by the European Union's Horizon 2020 Research and Innovation Program (Grant agreement No. 669947) and the Danish National Research Foundation through the Danish Center for Hadal Research (DNRF145) and the Danish Center for Electromicrobiology (DNRF136). Sample collection was supported by HYDRA Marine Sciences GmbH (Bühl, Germany), PULZ im Rieselfeld (Freiburg, Germany), and MACRORE (European Union's Horizon 2020 Research and Innovation Program (Grant agreement No. 654182; ENVRIplus)). We would like to thank the following colleagues and friends for their kind and active engagement in collecting samples: Kathrin Graffe, Nicole Ehlers, Tillman Keller, Jutta Drees, Jasper Dammann, Fabian Seredszus, Stefanie Tenten, Georg Supp, Herdís G. R. Steinsdóttir, Mon O. Yee, Hans F. Hansen, Michael W. Hansen, Lorenzo Rovelli, Irina-Elena Antonescu, Irene Olivé, Kelsey I. Miller, Marco Bonaglia, Artur Fink, Miriam Weber, Frank Wenzhöfer, Marit van Erk, and Elisa Merz. Microalgal isolates were kindly provided by Olga Kourtchenko (Gothenburg University Marine Algae Culture Collection, GUMACC), Tina Trautmann, Jan-Hendrik Hehemann, Daniel Doherty, and Hans F. Hansen. The technical support by Erik Laursen, Susanne Nielsen, Anja Niclas, and Gaby Eickert-Groetzschel is acknowledged.

Author contributions

P.S. designed the study, collected and analyzed samples, analyzed and interpreted data, and conceived and wrote the manuscript. A.K., A.S.C.H.R., R.N.G., and D.B. interpreted data and wrote the manuscript. C.S., M.B.L., and A.G. analyzed samples and data and contributed to manuscript preparation and editing. R.A., M.A., K.A., S.B., J.D., B.F.C., E.G.R., M.H., U.J., A.M., M.M., R.P., T.S.T., A.S., and D.S. collected and processed samples and contributed to manuscript preparation and editing.

Competing interests

The authors declare no competing interests.

Additional information

Supplementary information The online version contains supplementary material available at https://doi.org/10.1038/s43247-022-00485-8.

Correspondence and requests for materials should be addressed to Peter Stief.

Peer review information *Communications Earth & Environment* thanks Daniel Thornton, Alex Poulton, and the other, anonymous, reviewer(s) for their contribution to the peer review of this work. Primary handling editors: Clare Davis.

Reprints and permission information is available at http://www.nature.com/reprints

Publisher's note Springer Nature remains neutral with regard to jurisdictional claims in published maps and institutional affiliations.

Open Access This article is licensed under a Creative Commons Attribution 4.0 International License, which permits use, sharing, adaptation, distribution and reproduction in any medium or format, as long as you give appropriate credit to the original author(s) and the source, provide a link to the Creative Commons license, and indicate if changes were made. The images or other third party material in this article are included in the article's Creative Commons license, unless indicated otherwise in a credit line to the material. If material is not included in the article's Creative Commons license and your intended use is not permitted by statutory regulation or exceeds the permitted use, you will need to obtain permission directly from the copyright holder. To view a copy of this license, visit http://creativecommons.org/licenses/by/4.0/.

© The Author(s) 2022